AUT Journal of Electrical Engineering

AUT J. Elec. Eng., 50(1)(2018)67-74
DOI: 10.22060/eej.2017.12153.5048

Fast Transient Hybrid Neuro-Fuzzy Controller for STATCOM During Unbalanced Voltage Sags

R. Zaheri, A. Khoshsaadat, J. S. Moghani*, M. Abedi

Department of Electrical Engineering, Amirkabir University of Technology, Tehran, Iran

ABSTRACT: A static synchronous compensator (STATCOM) is generally used to regulate voltage and improve transient stability in transmission and distribution networks. This is achieved by controlling reactive power exchange between STATCOM and the grid. Unbalanced sags are the most common type of voltage sags in distribution networks. A static synchronous compensator (STATCOM) is generally used to maintain voltage and improve transient stability. This is achieved by regulating reactive power exchange between compensator device and grid. In this paper, A hybrid neuro-fuzzy current controller for STATCOM control is proposed. The controller has minimum mass of calculations. Learning process is carried out by an improved supervisory error-back propagation (SEBP) method instead of usual EBP algorithm. This results in better performance and efficiency and leads to a robust model with fast transient capability. The model is developed in MATLAB/SIMULINK environment. STATCOM operation during scenarios of balanced and unbalanced voltage sags is studied. Performance is compared with the operation of a conventional proportional-resonant controller. The results show faster dynamic and better capability of neuro-fuzzy controller in responding to voltage sag occurrences.

Review History:
Received: 12 November 2016
Revised: 3 September 2017
Accepted: 11 October 2017
Available Online: 1 December 2017

Keywords:
Static synchronous compensator
Voltage sag
Neuro-fuzzy systems

1- Introduction

In power grids, different electrical loads generate or absorb varying amounts of reactive power. If the reactive power balance is not held at all times, it might result in voltage sags or swells that exceed the acceptable variation of voltage amplitude and phase. It should be noted that multiple statistical analyses show unbalanced sags are more likely to happen [1-2].

A static synchronous compensator (STATCOMs) is a member of FACTS devices family. It is essentially a voltage source power converter connected parallel to AC network. It can either inject or absorb reactive power to maintain voltage. Installing a STATCOM at a proper point in power grids results in a better and smoother voltage profile even during severe voltage drops.

STATCOM technology has been thoroughly examined and investigated in the literature [3-21]. Design and implementation of new topologies in order to improve the performance are reported in [3-7]. One of the main topics regarding STATCOM is the implementing of different control methods. Various control methods based on current control strategy are reported in [5], [8-21].

In [7-12], the control scheme is implemented using PI controllers. The major shortcoming of these controllers is the inability of PI in following sinusoidal references without steady-state error. Thus, the controller operation is carried out in dq-frame using Park transformation or a feed-forward term from grid voltage is used to improve the system dynamics.

In [13-15], PI controllers are replaced with proportional-resonant (PR) controllers. PR controllers can handle sinusoidal references with ease, thus eliminating the need for using Park transformation. This method lowers the required processing power and overall bill of materials.

In recent years, many advances have been made in the field of intelligent control. Fuzzy systems and artificial neural networks are two major categories for implementing system controllers. Studies show that neural network theory can be used to determine the parameters of fuzzy systems. The results in a hybrid intelligent system [23-28]. The hybrid system holds learning capability of a artificial neural network and a fuzzy system's ability to deal with uncertainties in a system [25]. In this paper, a hybrid neuro-fuzzy controller for STATCOM is proposed.

The controller is comprised of two major parts: A) a four-layer neural network in accordance with four parts of a fuzzy system and B) simple fuzzy IF-THEN rules. The artificial neural network is responsible for creating a complete submodule of the fuzzy system. EBP (Error Back-Propagation) technique can be used to train the network. In this study, a linear supervisory procedure is also implemented. The success of this particular method is demonstrated in [23].

The present paper is divided into the following sections. Section 2 provides a short introduction of fuzzy systems and artificial neural networks. Electrical system configuration is presented in Section 3. Basics of the control scheme and current reference signals are given in Section 4. Section 5 describes the design procedure and learning process of the neuro-fuzzy control system. Simulation results are obtained in MATLAB/SIMULINK environment and presented in Section 6. Finally, concluding remarks are presented in section 7.

The corresponding author; Email: moghani@aut.ac.ir

2- Hybrid Neuro-Fuzzy System

In recent years, many advances have been made in the field of intelligent control. Fuzzy systems and artificial neural networks are two major categories for implementing control systems. The fuzzy systems are used to deal with vagueness or uncertainty in a control unit. Membership functions with normalized values are used in fuzzy logic control to handle control issues like non-linear characteristics and parameter disturbances. The fuzzy systems have flexible and intuitive knowledge-based design, simpler end-user interpretation. Also, they combine regulation algorithms and logic reasoning, which allows for implementing integrated control systems. But, in this method a compromise between accuracy and readability is inevitable and some real-world implementations are just equivalent to lookup-table interpolation schemes [22]. The artificial neural networks use processing units to model biological neurons. The relationship between these neurons is defined as a weight which can be trained in an online or offline process or a combination of the both [25]. The main characteristics of the artificial neural networks are their learning capability, resulting in modified weights to reach an optimum input-output relationship. Generalization capacity, parallel processing, and robustness to disturbances are the other advantages of the artificial neural networks.

Artificial neural networks and fuzzy systems can be combined to form a hybrid system. The new system combines the learning capability of a neural network and a fuzzy system's ability to deal with uncertainties in a system. It is called a neuro-fuzzy system. In a neuro-fuzzy system, each unit of the fuzzy system (fuzzifier, rule base, inference engine and defuzzifier) is implemented by a layer of the artificial neural network. Each layer consists of a number of neurons that are in accordance with the number of fuzzy areas [25-26].

3- Power System Configuration

The diagram of the studied power system is shown in Fig. 1. It is comprised of STATCOM, output filter and Thevenin equivalent of electrical grid.

The STATCOM model consists of a two-level three-phase voltage source converter and a DC link Capacitor. The LCL filter is used as an output filter for STATCOM. L_i and L_o are converter side and grid side inductances, respectively. C_f is the filter capacitor. The electrical grid is modeled using the three-phase voltage source V_{grid} and R_{grid}, L_{grid} as a grid impedance. STATCOM is connected to the point of common coupling (PCC).

4- Control System

The block diagram of the control system is shown in Fig 2. It consists of a voltage sequence analyzer, inner voltage control loop, outer current control loop, and space vector modulator. Control system uses PCC voltage and converter side current as inputs. It is shown in [29-30] that the sampling of converter side current instead of grid side current's results in a more robust system. An enhanced version of the current control strategy is implemented in αβ reference frame.

Voltage sequence analyzer is used to extract the positive and negative components of PCC voltage. These components are supplied to control loops as the primary inputs. Multiple voltage sequence extraction methods are reported in the literature. In this study, the method discussed in [31-32] is used. Positive and negative voltage components are extracted in αβ reference frame as follows:

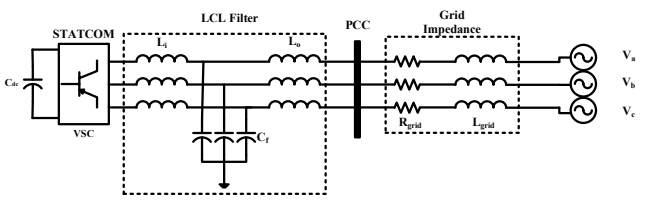

Fig. 1. Power system configuration

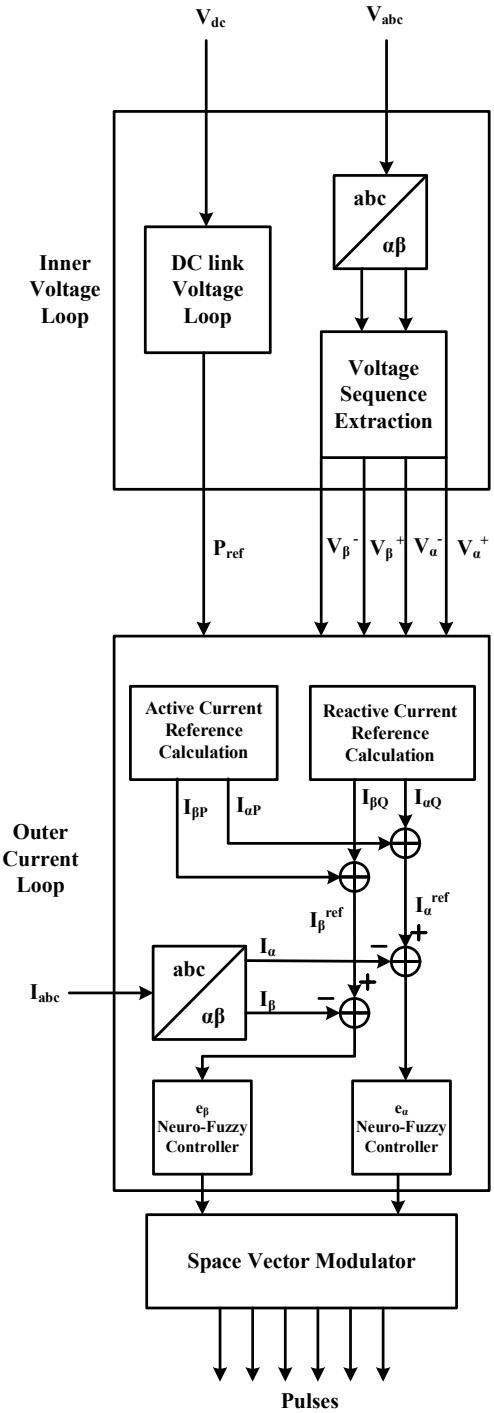

Fig. 2. STATCOM control system

$$v_\alpha = v_\alpha^+ + v_\alpha^- \quad (1)$$

$$v_\beta = v_\beta^+ + v_\beta^- \quad (2)$$

The symmetrical voltage components are defined as:

$$v_\alpha^+ = V^+ \cos\left(\omega t + \varphi^+\right) \quad (3)$$

$$v_\beta^+ = V^+ \sin\left(\omega t + \varphi^+\right) \quad (4)$$

$$v_\alpha^- = V^- \cos\left(\omega t + \varphi^-\right) \quad (5)$$

$$v_\beta^- = V^- \sin\left(\omega t + \varphi^-\right) \quad (6)$$

where V^+ and V^- are amplitudes of total positive and negative components, respectively. ω is the angular frequency and ϕ^+ and ϕ^- are initial phases of components.

During unbalanced voltage sags, the current is heavily distorted by harmonics. By using the following active current references, harmonic distortion is considerably reduced [13-15]:

$$i_{\alpha P}^{ref} = \frac{2}{3}\frac{v_\alpha^+}{\sqrt{\left(v_\alpha^+\right)^2 + \left(v_\beta^+\right)^2}} P_{ref} = \frac{2}{3}\frac{v_\alpha^+}{\sqrt{\left(V^+\right)^2}} P_{ref} \quad (7)$$

$$i_{\beta P}^{ref} = \frac{2}{3}\frac{v_\beta^+}{\sqrt{\left(v_\alpha^+\right)^2 + \left(v_\beta^+\right)^2}} P_{ref} = \frac{2}{3}\frac{v_\beta^+}{\sqrt{\left(V^+\right)^2}} P_{ref} \quad (8)$$

where P_{ref} is the active power reference. It is generated by a conventional PI controller in dc voltage loop. The following reactive current references [14-15] also reduce harmonic distortions:

$$i_{\beta Q}^{ref} = \frac{2}{3}\frac{-k_q v_\alpha^+ - \left(1-k_q\right)v_\alpha^-}{k_q\left(V^+\right)^2 + \left(1-k_q\right)\left(V^-\right)^2} Q_{ref} \quad (9)$$

$$i_{\alpha Q}^{ref} = \frac{2}{3}\frac{k_q v_\beta^+ + \left(1-k_q\right)v_\beta^-}{k_q\left(V^+\right)^2 + \left(1-k_q\right)\left(V^-\right)^2} Q_{ref} \quad (10)$$

where Q_{ref} is the reactive power reference and k_q is the control gain. k_q specifies the portion of reactive power that is transferred through positive sequence component. It is chosen in the range of $0 \le k_q \le 1$, where $k_q = 0$ represents an injection of reactive power via negative sequence only while $k_q = 1$ is used for injection via a positive sequence. The following current references are derived in [14]. The relations (11) and (12) have the advantage of directly involving a current set point of STATCOM.

$$i_{\alpha Q}^{ref} = \frac{2}{3}\frac{k_q v_\beta^+ + \left(1-k_q\right)v_\beta^-}{\sqrt{k_q^2 - 2k_q\left(1-k_q\right)\cos_{\min} + n^2\left(1-k_q\right)^2}} \frac{I_{ref}}{V^+} \quad (11)$$

$$i_{\beta Q}^{ref} = \frac{2}{3}\frac{-k_q v_\alpha^+ - \left(1-k_q\right)v_\alpha^-}{\sqrt{k_q^2 - 2k_q\left(1-k_q\right)\cos_{\min} + n^2\left(1-k_q\right)^2}} \frac{I_{ref}}{V^+} \quad (12)$$

where the I_{ref} is the current set point and the function cos_{min} denotes:

$$\cos_{\min} = \min\left(\cos x\right) \quad (13)$$

with x being phases a, b or c. In the relations (11) and (12), n represents the voltage unbalance factor. It is defined as the ratio of negative sequence component to the positive sequence component of voltage. Usually, $n<0.02$, but during voltage sags, it can rise up to 0.4 or even higher [1-2].

$$n = \frac{V^-}{V^+} \quad (14)$$

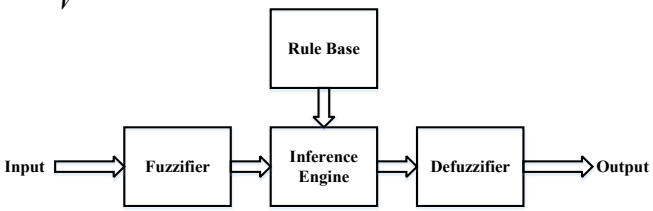

Fig. 3. The general structure of the fuzzy system

5- Neuro-Fuzzy Controller Design

A fuzzy system consists of four major components as shown in Fig 3. Fuzzifier maps the crisp input to fuzzy plain. Rule base contains the database of fuzzy inference system. Inference engine uses interpretations that exist in the rule base to perform fuzzy inference operation. Fuzzy data is reverted back to the crisp output by defuzzifier [22],[25].

In this study, a membership function with three sets of input

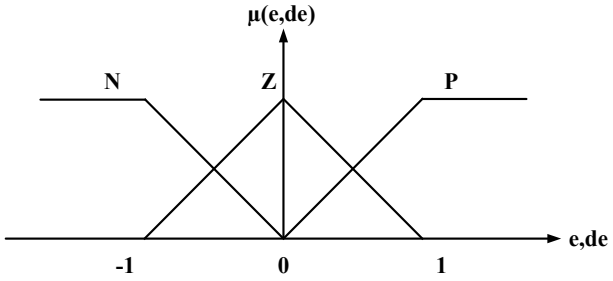

Fig. 4. Triangular membership function

variables N, Z, P is used which represent negative, zero, and positive inputs, respectively. Employing the minimum number of fuzzy rules minimizes the mass of calculations in the fuzzy systems [22],[25]. The triangular membership function is used as a fuzzifier. The triangular function has a minimum mass of calculations compared to other membership functions such as Bell-shape, Gaussian, etc. the error signal and its time derivative are shown in Fig. 4 in fuzzied framework.

Table. 1 presents the fuzzy inference table of the neuro-fuzzy system. Considering one of three fuzzy states is always designated to each input signal, fuzzy rule base contains nine rules in total.

Table 1. Fuzzy inference table

de / e	N	Z	P
N	NB	NS	Z
Z	NS	Z	PS
P	Z	PS	PB

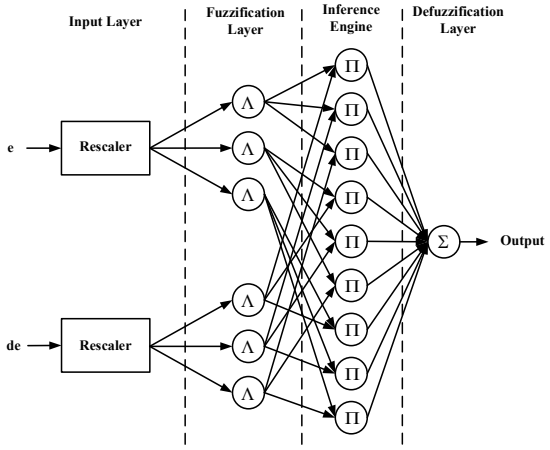

Fig. 5. Neuro-fuzzy control system

The structure of the proposed neuro-fuzzy control system is shown in Fig. 5.

The current error signals are calculated as follows:

$$e_\alpha = i_\alpha^{ref} - i_\alpha \tag{15}$$

$$e_\beta = i_\beta^{ref} - i_\beta \tag{16}$$

These signals are used as the crisp input for the neuro-fuzzy control system. The system consists of four layers: an input layer, fuzzification layer, inference layer and defuzzification layer.

Input layer: The input is rescaled in a predefined range that membership functions use. It is done in order to prevent input signals from entering the saturation zone of the membership function. For this layer:

$$Y_i^1 = k_i^1 x_i^1, \qquad i = 1,2. \tag{17}$$

The neural network contains a 2-6-9-1 node structure in accordance with layers. For each layer, xi parameter represents the i-th input of that layer, while outputs are expressed by Yi variables.

Fuzzification layer: Every node in this layer performs fuzzification with a triangular membership function. Fuzzy outputs are as follows:

$$Y_i^2 = T_j\left(x_i^2\right), \qquad i, j = 1,2,3, \tag{18}$$

where T is the triangular function.

Inference layer: Nodes of this layer perform the fuzzy AND operation as follows:

$$Y_i^3 = Y_j^2 Y_k^2, \qquad i = 1,2,...,9,\ j,k = 1,2,3. \tag{19}$$

Inputs of this layer represent the firing strength of i-th rule.

Defuzzification layer: A single node computes the normalized summation of all incoming signals to produce the defuzzified output. A mass of gravity method is used as a method to generate the crisp output as given in the following,

$$Y^4 = R = \frac{\sum_{i=1}^{9} w_i^4 Y_i^3}{\sum_{i=1}^{9} w_i^4} \tag{20}$$

where w_i is the weight of 4-th layer inputs. Training artificial neural networks are essential for properly updating the weights. In this study, the technique EBP is adopted for updating the weights. In this technique, weights are modified by passing the output error signal through the previous layers. It should be noted that EBP technique is one of the techniques that are sensitive to disturbance and learning rate coefficient [27]. By adding a correction coefficient to the EBP algorithm, the learning process can be improved. This coefficient acts as a supervisor and increases the convergence rate of the neuro-fuzzy system [23]. The supervisor demonstrates how close to the ideal output the network's output has become. It is modeled as a PD control system:

$$R = P.e + D.de \tag{21}$$

where P and D are supervisor coefficients. To train the artificial neural network with a linear PD supervisor, a cost function is proposed:

$$C(w_i) = \frac{1}{2} R^2. \tag{22}$$

w_i should be adjusted in the direction of the negative gradient of $C(w_i)$. Thus, for the last layer, we have:

$$\Delta w_i \propto -\frac{\partial C}{\partial w_i} \tag{23}$$

$$\Rightarrow \Delta w_i \propto -\frac{\partial C}{\partial R}\frac{\partial R}{\partial y}\frac{\partial y}{\partial x}\frac{\partial x}{\partial w_i}, \tag{24}$$

$$\Rightarrow \Delta w_i \propto -R\frac{\partial R}{\partial y}\frac{\partial y}{\partial x}\frac{\partial x}{\partial w_i}. \tag{25}$$

With attention to (21) and input-output function of the system, we have

$$\Delta w_i \propto \boldsymbol{R}\ \frac{\partial x}{\partial w_i} \tag{26}$$

With considering PD controller as a supervisor, online updating law is given by:

$$w_i^{new} = w_i^{old} + \eta R \frac{x_i^4}{\sum_{i=1}^{9} x_i^4} \tag{27}$$

where η is the learning rate coefficient of the neuro-fuzzy system. In order to minimize calculations and lower system complexity, the learning process is limited to the last layer [28].

6- Simulation Results

STATCOM model and the control system have been developed using SimPowerSystems toolbox from MATLAB/ SIMULINK software package. The supervisor coefficients are determined by trial and error as follows:

P=0.000002, D=96, k_1=0.000001,
k_2=0.00008, k_3=2, k_4=1200000

The learning rate coefficient is chosen as $\eta=0.6$. STATCOM performance is investigated under a set of three different voltage sags. At each test, voltage sag occurs at $t=300ms$ with a duration of $200ms$. Voltage and current waveforms

for each scenario are shown. In order to demonstrate the improved dynamics of proposed controller, the operation of neuro-fuzzy control system vs. conventional PR controller is investigated.

Balanced three-phase sag: Table. 2 shows the voltage characteristics before and after sag occurrence. Vector diagram of voltages is also shown in Fig. 6. RMS voltage variation of phase A for PR and neuro-fuzzy controllers are displayed in Fig. 7.
A balanced sag with an amplitude of *0.15pu* occurs at *t=300ms*. Fig. 7 compares the dynamical performance of controllers. Although, both controllers managed to maintain good voltage profile during sag, neuro-fuzzy control system was superior. PCC voltage drops to 0.86pu by using PR controller. By implementing the neuro-fuzzy controller, minimum voltage during sag is only *0.91pu*. This shows a *5%* improvement over the conventional controller.
After the fault is removed, the proposed controller again shows a better transient response. The maximum voltage overshoot after sag removal is *1.062pu* for PR controller and *1.046pu* for the neuro-fuzzy controller.

Table 2. Characteristics for the balanced three-phase sag

Three-phase sag	Before sag (pu)	After sag (pu)
V_a	1∠0°	0.85∠0°
V_b	1∠–120°	0.85∠–120°
V_c	1∠120°	0.85∠120°

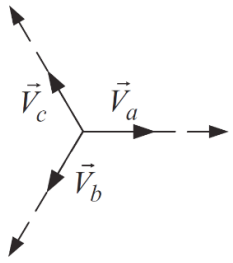

Fig. 6. Balanced three-phase voltage sag vector diagram

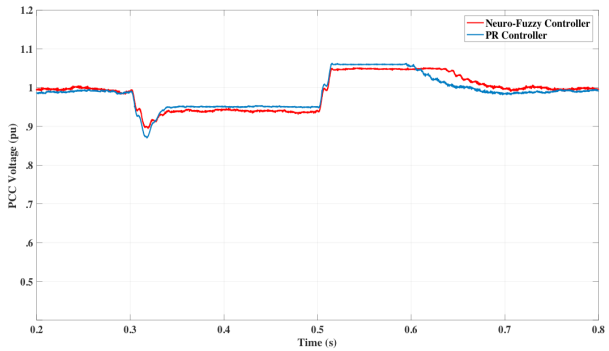

Fig. 7. RMS voltage variation of phase A during three-phase voltage sag

Unbalanced single-phase-to-ground sag: The voltage characteristics before and after sag occurrence are presented in Table. 3. The vector diagram of voltages is also illustrated in Fig. 8. RMS voltage variations for PR and neuro-fuzzy controllers are shown in Fig. 9.
An unbalanced sag with an amplitude of *0.5pu* occurs at *t=300ms* in phase A. RMS voltage variation of phase A for both controllers is shown in Fig. 9. It is clear that the proposed controller is superior in terms of voltage support during sag. PCC voltage has a minimum value of *0.6pu* while PR controller is applied. By employing the neuro-fuzzy controller, the minimum voltage rises to *0.63pu* during sag. This shows a *3%* improvement over the conventional controller.
After fault removal, the proposed controller shows a better transient response. The maximum voltage overshoot after sag removal is *1.06pu* for PR controller, while it is limited to *1.049pu* for the neuro-fuzzy controller.

Table 3. Characteristics of unbalanced single-phase-to-ground sag

Single-phase-to-ground sag	Before sag (pu)	After sag (pu)
V_a	1∠0°	0.5∠0°
V_b	1∠–120°	1∠–120°
V_c	1∠120°	1∠120°

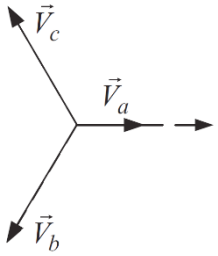

Fig. 8. Unbalanced single-phase-to-ground voltage sag vector diagram

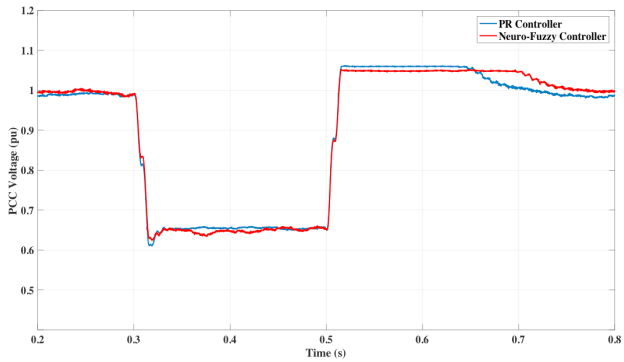

Fig. 9. RMS voltage variation of phase A during single-phase-to-ground voltage sag

Unbalanced two-phase-to-ground sag: Table 4 shows the voltage characteristics before and after sag occurrence. The vector diagram of voltages during this sag is also shown in Fig. 10. RMS voltage of phase B and phase C for PR and neuro-fuzzy controllers are displayed in Fig. 11 and Fig. 12, respectively.

RMS voltage of phase B drops to 0.576pu when PR controller is employed. By using neuro-fuzzy controller, voltage is kept is at 0.653pu during sag. Phase C voltage variations during sag are similar. Neuro-fuzzy controller maintains RMS voltage at 0.64pu during fault, while voltage drops to 0.62pu when PR controller is used.

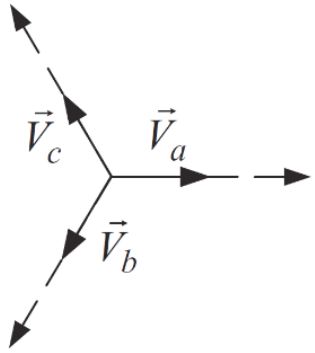

Fig. 10. Unbalanced two-phase-to-ground voltage sag vector diagram

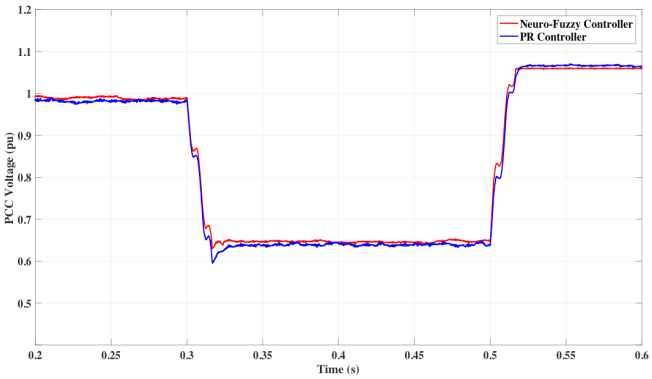

Fig. 11. RMS voltage variations for phase B during two-phase-to-ground voltage sag

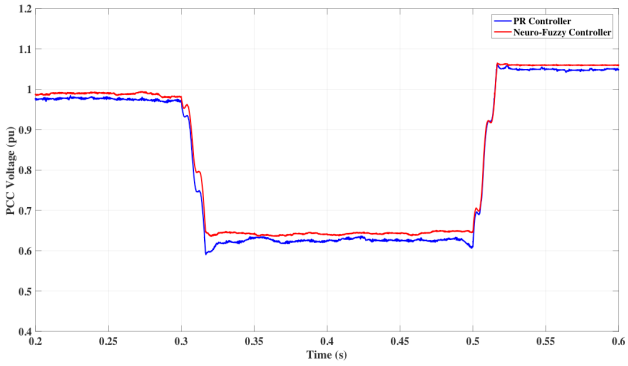

Fig. 12. RMS voltage variations for phase C during two-phase-to-ground voltage sag

Table 4. Characteristics of the unbalanced two-phase-to-ground sag

Two-phase-to-ground sag	Before Sag (pu)	After Sag (pu)
V_a	$1\angle 0°$	$1\angle 0°$
V_b	$1\angle -120°$	$0.5\angle -150°$
V_c	$1\angle 120°$	$0.5\angle 150°$

In order to demonstrate the improved dynamics of the proposed controller, injected current signals rise times to 97% of the nominal value have been measured. The comparison between the proposed and conventional PR controllers is shown in Table. 5. The results show the proposed controller responds faster to sag occurrence than the conventional PR controller.

Table 5. Comparison between transient capability of neuro-fuzzy and PR controllers

Fault Type	Neuro-fuzzy controller response time (s)	PR controller response time (s)
Three-phase sag	0.023	0.032
Single-phase-to-ground sag	0.040	0.047
Two-phase-to-ground sag	0.030	0.035

7- Conclusion

In this paper, an adaptive and robust hybrid neuro-fuzzy controller was proposed for STATCOM control during balanced and unbalanced voltage sags. A four-layer artificial neural network was used in order to implement the neuro-fuzzy system with the minimum fuzzy rules and computational burden. An improved Error-Back Propagation method was exploited with Otimum updating rules. Operation of the controller during three types of unbalanced voltage sags (single-phase, phase-to-phase and two-phase-to-ground) was simulated in MATLAB/SIMULINK. The improved dynamical response of the proposed controller compared to conventional PR controller was illustrated. The neuro-fuzzy controller outperforms in improving voltage profile during faults and minimizing overshoot after the fault is cleared.

References

[1] Yalienkaya, G., Bollen, M.H.J. and Crossley, P.A., Characterization of Voltage Sags in Industrial Distribution System, IEEE Transactions on Industry Applications, 34(4) (1999) 682-688.

[2] Bollen, M.H., Algorithms for characterizing measured three-phase unbalanced voltage dips, IEEE Transactions on Power Delivery, 18(3) (2003) 937-944.

[3] Singh, B., Saha, R., Chandra, A. and Al-Haddad, K., Static synchronous compensators (STATCOM): a review,

IET Power Electronics, 2(4) (2009) 297-324.

[4] Bindal, R.K., A Review of Benefits of FACTS Devices in Power system, International Journal of Engineering and Advanced Technology (IJEAT), 3(4) (2014) 105-108.

[5] Zafari, A. and Jazaeri, M., STATCOM systems in distribution and transmission system applications: a review of power-stage topologies and control methods. International Transactions on Electrical Energy Systems, 26(2) (2016) 323-346.

[6] Slepchenkov, M.N., Smedley, K.M. and Wen, J., Hexagram-converter-based STATCOM for voltage support in fixed-speed wind turbine generation systems, IEEE Transactions on Industrial Electronics, 58(4) (2011) 1120-1131.

[7] Pulikanti, S.R. and Agelidis, V.G., Hybrid flying-capacitor-based active-neutral-point-clamped five-level converter operated with SHE-PWM, IEEE Transactions on Industrial Electronics, 58(10) (2011) 4643-4653.

[8] Sharma, P. and Bhatti, T.S., Performance investigation of isolated wind–diesel hybrid power systems with WECS having PMIG, IEEE Transactions on Industrial Electronics, 60(4) (2013) 1630-1637.

[9] Anand, S., Fernandes, B.G. and Chatterjee, K., DC voltage controller for asymmetric-twin-converter-topology-based high-power STATCOM, IEEE Transactions on Industrial Electronics, 60(1) (2013) 11-19.

[10] Han, C., Huang, A.Q., Baran, M.E., Bhattacharya, S., Litzenberger, W., Anderson, L., Johnson, A.L. and Edris, A.A., STATCOM impact study on the integration of a large wind farm into a weak loop power system, IEEE Transactions on Energy Conversion, 23(1) (2008) 226-233.

[11] Song, W. and Huang, A.Q., Fault-tolerant design and control strategy for cascaded H-bridge multilevel converter-based STATCOM, IEEE Transactions on Industrial Electronics, 57(8) (2010) 2700-2708.

[12] Sepulveda, C.A., Muñoz, J.A., Espinoza, J.R., Figueroa, M.E. and Melin, P.E., All-on-chip dq-frame based D-STATCOM control implementation in a low-cost FPGA, IEEE Transactions on Industrial Electronics, 60(2) (2013) 659-669.

[13] Camacho, A., Castilla, M., Miret, J., Vasquez, J.C. and Alarcón-Gallo, E., Flexible voltage support control for three-phase distributed generation inverters under grid fault, IEEE Transactions on Industrial Electronics, 60(4) (2013) 1429-1441.

[14] Castilla, M., Miret, J., Camacho, A., Matas, J. and de Vicuña, L.G., Voltage support control strategies for static synchronous compensators under unbalanced voltage sags, IEEE Transactions on Industrial Electronics, 61(2) (2014) 808-820.

[15] Castilla, M., Miret, J., Camacho, A., de Vicuña, L.G. and Matas, J., Modeling and design of voltage support control schemes for three-phase inverters operating under unbalanced grid conditions, IEEE Transactions on Power Electronics, 29(11) (2014) 6139-6150.

[16] Molinas, M., Suul, J.A. and Undeland, T., Low voltage ride through of wind farms with cage generators: STATCOM versus SVC, IEEE Transactions on Power Electronics, 23(3) (2008) 1104-1117.

[17] Suul, J.A., Molinas, M. and Undeland, T., STATCOM-based indirect torque control of induction machines during voltage recovery after grid faults, IEEE Transactions on Power Electronics, 25(5) (2010) 1240-1250.

[18] Yazdani, A., Sepahvand, H., Crow, M.L. and Ferdowsi, M., Fault detection and mitigation in multilevel converter STATCOMs, IEEE Transactions on Industrial Electronics, 58(4) (2011) 1307-1315.

[19] Li, K., Liu, J., Wang, Z. and Wei, B., Strategies and operating point optimization of STATCOM control for voltage unbalance mitigation in three-phase three-wire systems, IEEE Transactions on Power Delivery, 22(1) (2007) 413-422.

[20] Lee, T.L., Hu, S.H. and Chan, Y.H., D-STATCOM with positive-sequence admittance and negative-sequence conductance to mitigate voltage fluctuations in high-level penetration of distributed-generation systems, IEEE Transactions on Industrial Electronics, 60(4) (2013) 1417-1428.

[21] Castilla, M., Miret, J., Camacho, A., Matas, J., Alarcón-Gallo, E. and de Vicuña, L.G., Coordinated reactive power control for static synchronous compensators under unbalanced voltage sags, Industrial Electronics (ISIE), 2012 IEEE International Symposium, (2012) 987-992.

[22] Albertos, P. and Sala, A., , September. Fuzzy logic controllers. Advantages and drawbacks, VIII International Congress of Automatic Control (3) (1998) 833-844.

[23] Khoshsaadat, A., Mosavi, M.R. and Moghani, J.S., A controller design with ANFIS architecture attendant learning ability for SSSC-based damping controller applied in single machine infinite bus system, Iranian Journal of Electrical and Electronic Engineering, 10(3) (2014) 212-222.

[24] Nauck, D., Klawonn, F. and Kruse, R., Foundations of neuro-fuzzy systems. John Wiley & Sons, Inc., (1997).

[25] Siddique, N. and Adeli, H., Computational intelligence: synergies of fuzzy logic, neural networks and evolutionary computing, John Wiley & Sons, (2013).

[26] Vieira, J., Dias, F.M. and Mota, A., April. Neuro-fuzzy systems: a survey, 5th WSEAS NNA International Conference on Neural Networks and Applications, Udine, Italia, (2004).

[27] Jang, J.S., Self-learning fuzzy controllers based on temporal backpropagation, IEEE Transactions on Neural Networks, 3(5) (1992) 714-723.

[28] Jazbi, S.A., Development of Emotional Learning Methods for Intelligent Control and its Industrial Applications, Dept. of EE engineering, (1998).

[29] Figueres, E., Garcerá, G., Sandia, J., Gonzalez-Espin, F. and Rubio, J.C., Sensitivity study of the dynamics

of three-phase photovoltaic inverters with an LCL grid filter, IEEE Transactions on Industrial Electronics, 56(3) (2009) 706-717.

[30] Liserre, M., Teodorescu, R. and Blaabjerg, F., Stability of photovoltaic and wind turbine grid-connected inverters for a large set of grid impedance values, IEEE Transactions on Power Electronics, 21(1) (2006) 263-272.

[31] Rodríguez, P., Luna, A., Candela, I., Mujal, R., Teodorescu, R. and Blaabjerg, F., Multiresonant frequency-locked loop for grid synchronization of power converters under distorted grid conditions, IEEE Transactions on Industrial Electronics, 58(1) (2011) 127-138.

[32] Luna, A., Rocabert, J., Candela, J.I., Hermoso, J.R., Teodorescu, R., Blaabjerg, F. and Rodríguez, P., Grid voltage synchronization for distributed generation systems under grid fault conditions, IEEE Transactions on Industry Applications, 51(4) (2015) 3414-3425.

Please cite this article using:

R. Zaheri, A. Khoshsaadat, J. S. Moghani, M. Abedi, Fast Transient Hybrid Neuro-Fuzzy Controller for STATCOM During Unbalanced Voltage Sags, AUT J. Elec. Eng., 50(1)(2018) 67-74.

DOI: 10.22060/eej.2017.12153.5048